Soft robot shape estimation with IMUs leveraging PCC kinematics for drift filtering

Stella, Francesco; Santina, Cosimo Della; Hughes, Josie

DOI
10.1109/LRA.2023.3339063

Publication date
2024

Document Version
Final published version

Published in
IEEE Robotics and Automation Letters

Soft Robot Shape Estimation With IMUs Leveraging PCC Kinematics for Drift Filtering

Francesco Stella, Cosimo Della Santina, *Senior Member, IEEE*, and Josie Hughes, *Member, IEEE*

***Abstract*—The control possibilities for soft robots have long been hindered by the need for reliable methods to estimate their configuration. Inertial measurement units (IMUs) can solve this challenge, but they are affected by well-known drift issues. This letter proposes a method to eliminate this limitation by leveraging the Piecewise Constant Curvature model assumption. We validate the reconstruction capabilities of the algorithm in simulation and experimentally. To this end, we also present a novel large-scale, foam-based manipulator with embedded IMU sensors. Using the filter, we bring the accuracy in IMU-based reconstruction algorithms to 93% of the soft robot's length and enable substantially longer measurements than the baseline. We also show that the proposed technique generates reliable estimations for closed-loop control of the robot's shape.**

***Index Terms*—Calibration and identification, modeling, control, and learning for soft robots, soft sensors and actuators.**

I. Introduction

CONTINUUM soft robotic platforms [1] promise to revolutionize fields where safety and robustness to uncertainty are paramount, for example enabling human-robot interaction in industry 4.0, agri-food, and medicine. To bridge the gap between labs and the real world, advances in embedded control of soft structures are needed [2], [3]. This in turn requires knowing the robot's state. However accurately measuring and reconstructing the shape of a soft robot without relying on exteroceptive sensing techniques is an open research problem [4].

Solving this challenge requires novel sensing modalities and algorithms. The sensing should be designed so as not to compromise the deformation capabilities of the robot [5], [6], and the algorithms should compensate for potential issues in the novel sensing modalities and seek the correct trade-off between computational complexity and accuracy of reconstruction. Numerous sensing modalities have been proposed based on magnetic [6], resistive [7], optical [8], and visual [9] technologies. Inertial measurement units (IMUs) are a promising solution as they are compact, can be easily integrated into existing soft robot designs, and provide high-frequency data. In [10], an IMU-based reconstruction algorithm based on the Piecewise Constant Curvature (PCC) assumption was first proposed. Since then, the methodology has been used for disturbance observation [11], has been combined with visual information [12], and augmented with Kalman filtering [13]. Recently, [14] proposed a method to approximate the pose of soft structures with a series of rigid links by integrating the measurements of multiple IMU readings.

Notwithstanding the success of this approach, the drift arising from the integration of IMU measurements still significantly limits the performance and the maximum operation time of IMU-based reconstruction algorithms. In this work, we propose to solve this challenge with a novel filter, which exploits kinematic[1] models of continuum soft robots to estimate and remove the drift occurring on IMUs, ultimately resulting in accurate and driftless reconstructions of soft robots' shape. In

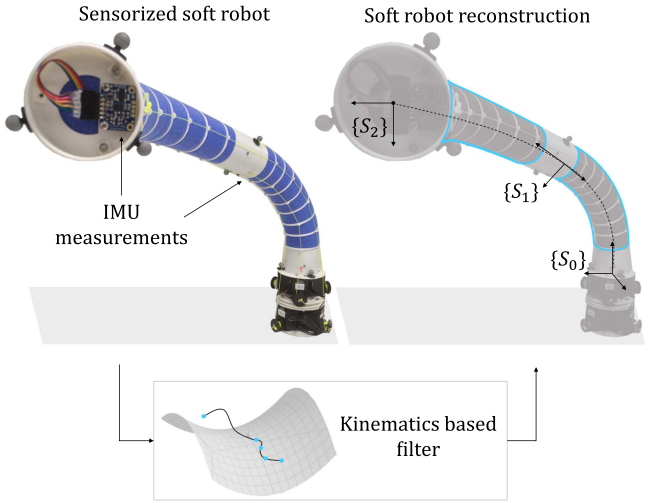

Fig. 1. Pictorial representation of the pipeline proposed. The IMUs embedded in the soft continuum arm are filtered to reconstruct the configuration of the structure, constraining the IMU signals to the manifold defined by the robot's kinematics.

Manuscript received 4 July 2023; accepted 20 November 2023. Date of publication 4 December 2023; date of current version 17 January 2024. This letter was recommended for publication by Associate Editor H. Hauser and Editor C. Laschi upon evaluation of the reviewers' comments. This work was supported by the EU's Horizon Europe Program from Project EMERGE under Grant Agreement number 101070918. *(Corresponding author: Francesco Stella.)*

Francesco Stella is with the CREATE Lab, EPFL, CH-1015 Lausanne, Switzerland, and also with the Department of Cognitive Robotics, Delft University of Technology, 2628 CD Delft, The Netherlands (e-mail: francesco.stella@epfl.ch).

Cosimo Della Santina is with the Department of Cognitive Robotics, Delft University of Technology, 2628 CD Delft, The Netherlands, and also with the Institute of Robotics and Mechatronics, German Aerospace Center (DLR), 82234 Wessling, Germany (e-mail: c.dellasantina@tudelft.nl).

Josie Hughes is with the CREATE Lab, EPFL, CH-1015 Lausanne, Switzerland (e-mail: josie.hughes@epfl.ch).

This letter has supplementary downloadable material available at https://doi.org/10.1109/LRA.2023.3339063, provided by the authors.

Digital Object Identifier 10.1109/LRA.2023.3339063

[1]We focus here on Piecewise Constant Curvature priors, but the proposed strategy can be easily generalized to more complex models [15].

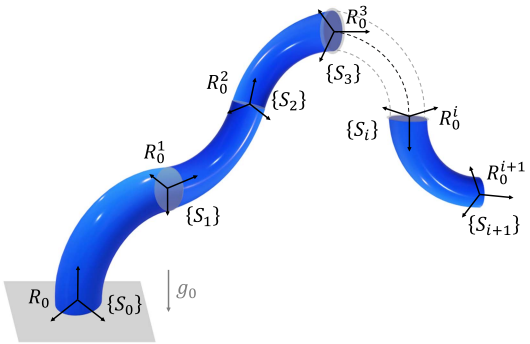

Fig. 2. Schematic representation of the ideal soft robot in an inertial frame of reference. The local frames S_i are represented as a triplet of orthonormal vectors, which are the image of the canonical basis of the inertial frame by the matrix R_0^i. The ellipses represented the cross-sections of the soft robot at its base and junctions.

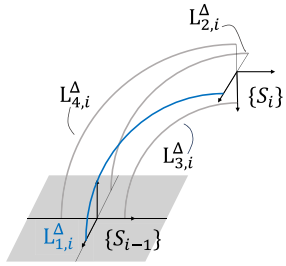

Fig. 3. Representation of the physical interpretation of the Lagrangian coordinates $q = [\Delta x, \Delta y]$. Δx represents the physical difference between $L^{\Delta}_{1,i}$ and $L^{\Delta}_{2,i}$. Similarly Δy represents the physical difference between $L^{\Delta}_{3,i}$ and $L^{\Delta}_{4,i}$. Thanks to the simple geometrical mapping shown in the center, it is possible to compute the tendon lengths as a function of $q = [\Delta x, \Delta y]$ and of the length of the central axis.

particular, the filter relies on an augmented model of the soft robot, which considers the drift and constraints of the IMU's data to the manifold defined by the soft robot's kinematics. While in [10] the errors of the IMUs signals with respect to the manifold were treated by solving an optimization problem, in the following we propose a novel algorithm that models the error, thus providing a physically informed estimation of the error and thus a drift-compensated soft robot reconstruction. We test the proposed algorithm in simulation and physical experiments. To this end, we also introduce a novel soft robotic manipulator with embedded proprioceptive capabilities which is on the meter scale. This is used to test the proposed algorithm in challenging experimental conditions. Fig. 1 shows this system and a pictorial representation of the proposed strategy. To summarize, this article contributes to the state-of-the-art in sensing of soft continuum structures with the following:

- A model-based reconstruction algorithm for continuum robot arms based on IMU readings (pre-filtered via a Mahony filter [16]), which estimates and compensates for the drift in the sensor's signal.
- A comparison of the filter's performance with state-of-the-art IMU-based algorithms and its validation in a control loop.
- The design and experimental validation of a large-scale, foam-based, soft manipulator with embedded proprioceptive sensing.

After a detailed statement of the problem and a mathematical definition of the drift (Section II), Section III presents the new filter. Section V introduces the experimental setup and a detailed description of the measurement system together with the design of the novel soft robot. We present simulation and experimental results in Sections IV and VI respectively, and we conclude by presenting a closed loop control algorithm and its experimental validation in Section VII.

II. Problem Statement

The proposed method is developed for a soft continuum robot, schematically represented in Fig. 2, composed of n incompressible flexible segments connected in series. We assume that an IMU is connected at the end of each segment.

This section starts with specifying the kinematic model used in this work, to move then to discuss the technological limitations of using IMUs that we aim to address with the novel kinematics-based filter.

A. Manipulator's Kinematic Model

In this work, we focus on a kinematic model based on the piecewise constant curvature assumption, shown in Fig. 3. Future work will be devoted to generalizing this strategy to more complex models. More specifically, we build on top of the improved piece-wise constant curvature parametrization presented in [17]. We consider n reference frames $\{S\}$ placed at the end of each segment plus one at the base, as in Fig. 2. Let R^i_{i-1} be the rotation matrix and t^i_{i-1} the translation mapping the reference frame at the base of the $i-$th segment to the one attached to its tip. The full pose of the i-th segment can be described by the Lagrangian coordinates $q = [\Delta_x, \Delta_y]$, intuitively related to the bending of the structure along the x and y axes respectively.

In particular, the orientation of frame $\{S_i\}$ expressed in the $\{S_{i-1}\}$ frame is fully specified by the rotation matrix $R^i_{i-1} =$

$$\begin{bmatrix} 1+\frac{\Delta^2_{x,i}}{\Delta^2_i}(1-c) & \frac{\Delta_{x,i}\Delta_{y,i}}{\Delta^2_i}(1-c) & \frac{-\Delta_{x,i}}{\Delta_i}s \\ \frac{\Delta_{x,i}\Delta_{y,i}}{\Delta^2_i}(1-c) & 1+\frac{\Delta^2_{y,i}}{\Delta^2_i}(1-c) & \frac{-\Delta_{y,i}}{\Delta_i}s \\ \frac{\Delta_{x,i}}{\Delta_i}s & \frac{\Delta_{y,i}}{\Delta_i}s & 1+(1-c) \end{bmatrix}, \quad (1)$$

and the position by the vector

$$t^i_{i-1}(\Delta_{\mathrm{x},i}, \Delta_{\mathrm{y},i}, L_i, s_i) = \frac{L_i}{\Delta^2_i}\begin{bmatrix} (1-\cos(s_i\Delta_i))\,\Delta_{\mathrm{x},i} \\ (1-\cos(s_i\Delta_i))\,\Delta_{\mathrm{y},i} \\ \sin(s_i\Delta_i)\,\Delta_i \end{bmatrix}, \quad (2)$$

with c and s being $\cos(s_i\Delta_i)$ and $\sin_i(s\Delta_i)$ respectively and $\Delta = \sqrt{\Delta^2_x + \Delta^2_y}$. The local coordinate along the segment is $s_i \in [0, 1]$, with 0 referring to the base and 1 to the tip. Due to the linear dependency between the Cartesian positions and the length of the structure L in (2), the error on the end effector position scales linearly with the length of the soft structure, making accurate control of large-scale structures challenging. Note that, due to the constant variation of orientation between subsequent segments, the IMU is not formally constrained to lie at the end of the segment and could be placed at any point along

the length of the segment, as parametrized by the variable s_i. Moreover, theoretically, IMUs do not need to be constrained to the central axis of the soft manipulator as the rotation matrix is equal along the section. This formulation allows expression of the orientation matrices of each frame $\{S_i\}$ with respect to the global frame as

$$R_0^i = \left(\prod_{j=i}^{1} R_{j-1}^j \right) R_0, \; i = 1, \ldots, N$$

with R_0 being the absolute orientation matrix of the frame $\{S_0\}$. In previous works, the rotation R_0^i was considered to match the orientation of the IMUs placed in each junction, resulting in a reconstruction accuracy of the end effector pose in the order of 10% the soft robot's length [10]. As presented below, this error in reconstruction accuracy is significantly affected by errors in the IMUs measurements, which tend to drift over time. In the following, we first present the properties of the drift phenomenon. Then we develop a filter able to compensate for the IMU drift by leveraging the kinematic properties of soft continuum structures.

B. Drift in IMU Data

Intertial Measurement Units (IMUs) allow for a high-frequency measurement of the sensor's orientation. Most IMUs come in integrated MEMS circuits composed of a gyroscope, measuring angular accelerations in the three axes, a magnetometer evaluating the direction of the magnetic field, and an accelerometer, measuring the linear accelerations of the sensor. Although standard methods to fuse these sources of information make the orientation data prone to drift over time, recently proposed techniques have proven able to reduce this problematic accumulation of error to a minimum. One successful method is to apply a stack of Mahony filters [16]. However, since this sensor fusion method requires the knowledge of the gravity vector and of the Earth's magnetic field to compensate for the rotation drift, knowing only one of these signals leads to a drift restricted to a particular sub-space of $\mathbb{R}^3$. In particular, the Mahony filter presented in [18] has shown that when the direction of the magnetic field is lost, the drift occurs only around the gravitational axis. In the same way, a saturation of the accelerometers leads to a loss of the direction of the gravity vector, which lets the drift occur around the Earth's magnetic field vector. Finally, the drift occurs even in a static case around the gravitational vector in long time measurements. We refer the reader to [19] for an experimental characterization of these behaviors on several off-the-shelf consumer-grade nine-axes motion sensors in composition with the embedded sensor fusion algorithm. Therefore, in addition to careful initial calibration, to ensure good measurements of the soft robot's state, the IMU needs to be re-calibrated regularly. As most soft robots are not subject to high accelerations, in this work, we aim at compensating for the drift happening:

- Due to a long-term accumulation of error around the local gravitational axis, as shown in Fig. 4(a).
- When the magnetometer data are lost. This malfunction results in abrupt changes in orientation around the gravitational axis, as shown in Fig. 4(b).

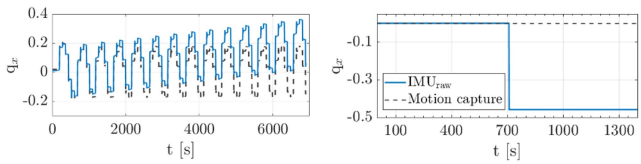

Fig. 4. Types of drift occurring in off-the-shelf IMU sensors (BNO055) when placed on the soft robotics structure presented in Section V.

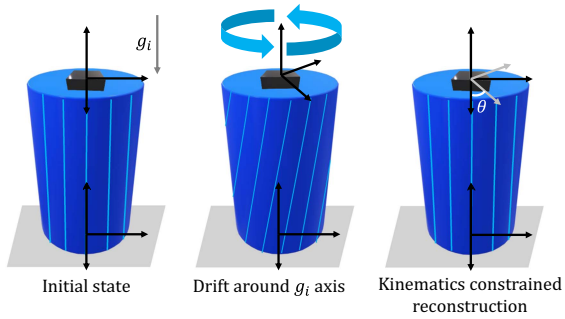

Fig. 5. Example of the behavior observed with augmented models. At the right, the IMU readings are just after calibration. In the center, the current state of the art in the reconstruction of the soft robot state when one of the IMU signals drifts around gravity. On the right, the correct reconstruction is achieved with the proposed drift-aware filter.

Consequently, in this work, we model the drift as a rotation of θ around the gravitational axis g. In the following, we express with $g = [g_x, g_y, g_z]$ the scalar components of the gravitational axis expressed in the relative IMU frame. Consequently, the drift in the IMU frame can be modeled as a rotation R_{drift} occurring around the g axis

$$\begin{bmatrix} \cos(\theta) - {g_x}^2\, c & -g_z\, s - g_x\, g_y\, c & g_y\, s - g_x\, g_z\, c \\ g_z\, s - g_x\, g_y\, c & \cos(\theta) - {g_y}^2\, c & -g_x\, s - g_y\, g_z\, c \\ -g_y\, s - g_x\, g_z\, c & g_x\, s - g_y\, g_z\, c & \cos(\theta) - {g_z}^2\, c, \end{bmatrix}, \quad (3)$$

with c and s being $(\cos(\theta) - 1)$ and $\sin(\theta)$ respectively.

This drift fundamentally limits the applicability of IMU-based proprioceptive sensing for soft robots, as they preclude the reconstruction accuracy over long-term measurements and deployment of soft structures into unsupervised environments.

III. Method: Kinematics Based Filter

The filter is a static filter applied sequentially to every orientation matrix measured by IMU (called $\tilde{R}_0^i$) that finds a projection into the soft robot frame S_i by correcting the drift angle θ around the estimated image of the local gravity vector $\tilde{g}_i$ in $\{S_i\}$. The estimate of θ_i and of $\tilde{g}_i$ are determined leveraging the manifold of PCC models, and consequently, its assumptions of negligible torsion and elongation. As an example of the filter's principle, consider a straight segment placed parallel to the gravitational axis, as shown in Fig. 5. In the initial state, just after calibration, both IMU's readings are compatible with the structure's state, and the full PCC state can be retrieved. However, as soon as a drift around the gravitational axis occurs, a PCC incompatible relative rotation between the top and bottom will be recorded.

In particular, the relative rotation $\tilde{R}^i_{i-1}$ would correspond to a torsion of the soft structure, as depicted in Fig. 5(b). However, one of the founding assumptions between PCC models is that the torsion of the structure is negligible. It is, therefore, possible to use the kinematics of the PCC space to detect and compensate for the drift in the IMU signal. As shown in Fig. 5(c), by performing the inverse kinematic on a drift-aware soft model, the structure is correctly reconstructed and the drift estimated.

A. An Augmented Drift-Aware Model

To compensate for the drift, we first need to develop a model which merges the kinematics of the soft structure, presented in Section II-A with the drifted IMU readings, as presented in Section II-B. Then, the kinematic estimator would exploit this model to estimate the drift and compute the correct value of $\Delta_{x,i}$ and $\Delta_{y,i}$ for each segment.

To compensate for the drift, first, the gravitational axis in the local IMU frame should be estimated. Without losing generality, we assume that the gravitational axis $\tilde{g}_0$ is known and parallel to the z axis of the world frame $\{S_0\}$, as presented in Fig. 2. In the local $\{S_i\}$ frame, a first estimation of the gravitational axis $\tilde{g}_i$ can be then computed using the soft robot's kinematics

$$\tilde{g}_i = \left(R_0^{i-1} R_{i-1}^{i-}\right)^{-1} g_0, \tag{4}$$

with R_{i-1}^{i-} being the filtered orientation at the precedent time-step. Another method to estimate $\tilde{g}_i$ for quasi-static applications is by directly reading the accelerometer's data from IMU. As the components of $\tilde{g}_i$ in the local frame have been estimated, the rotation R_{drift} modeling the drift can be then rewritten as a function of θ only. The orientation of the drifted IMU is consequently fully defined by the composition of the correct pose of the segment's end and the drift rotation R_{drift}.

$$\tilde{R}^i_0 = R^i_0(\Delta x, \Delta y) R_{\text{drift}}(\theta, \tilde{g}). \tag{5}$$

By including the drift in the model, it is possible to account for, estimate, and compensate for errors in the IMU signals which are out of the PCC manifold.

B. Drift Compensation

Given the formalization of the IMU state, the filter can be developed as a method to solve the inverse kinematic mapping

$$[\Delta x, \Delta y, \theta]_i = f\left(\tilde{R}^i_{i-1}\right). \tag{6}$$

However, given the complexity of (5), an analytical form of (6) can be found only for a few notable gravity orientations. For a general case, numerical methods are needed to find a solution. We propose to solve (6) with gradient descent on the augmented model presented in Section III-A. The drift compensation is achieved by sequentially compensating for the drift in each IMU signal, starting from the base of the robot until the end-effector of the robot. In this way, the knowledge of the orientation of the soft robot base is leveraged. Hence, for each segment, an initial estimate of the soft robot pose is achieved with

$$\Delta x = \frac{1}{2} \frac{\tilde{R}^i_{i-1}[3,1] - \tilde{R}^i_{i-1}[1,3]) \arccos\left(\tilde{R}^i_{i-1}[3,3]\right)}{\sin(\arccos(\tilde{R}^i_{i-1}[3,3])},$$

Algorithm 1: Manifold-Based Filter.

Input $\tilde{q}^i_0$, $\vec{g_i}$, for $i = 1, \ldots, N$
Output $\Delta_{x,i}$, $\Delta_{y,i}$, for $i = 1, \ldots, N$
$\epsilon \leftarrow$ Error tolerance
for i from 1 to n **do**
$\Delta x \leftarrow \frac{1}{2} \frac{\tilde{R}^i_{i-1}[3,1] - \tilde{R}^i_{i-1}[1,3]) \arccos(\tilde{R}^i_{i-1}[3,3])}{\sin(\arccos(\tilde{R}^i_{i-1}[3,3])}$
$\Delta y \leftarrow \frac{1}{2} \frac{\tilde{R}^i_{i-1}[3,2] - \tilde{R}^i_{i-1}[2,3]) \arccos(\tilde{R}^i_{i-1}[3,3])}{\sin(\arccos(\tilde{R}^i_{i-1}[3,3])}$
$\theta \leftarrow 0$
$q \leftarrow [\Delta x, \Delta y, \theta]$
$g_{\text{i}} = (\tilde{R}^i_0)^{-1} g_0$
while true
$\Delta R \leftarrow$ DisplacementFromManifold(q, g_i)
if $|\Delta x| \leq \epsilon$ **then**
return q
$J \leftarrow$ EvaluateJacobian(q, g_i)
$\Delta q \leftarrow J^\top (J J^\top)^{-1} \Delta R$
$q \leftarrow (q - \Delta q)$

$$\Delta y = \frac{1}{2} \frac{\tilde{R}^i_{i-1}[3,2] - \tilde{R}^i_{i-1}[2,3]) \arccos\left(\tilde{R}^i_{i-1}[3,3]\right)}{\sin(\arccos(\tilde{R}^i_{i-1}[3,3])}. \tag{7}$$

while the drift at the start of the measurement is initially estimated as 0. The local gravitational axis is evaluated with (4). This initial estimate is hence mapped into the manifold of (5). To do so, a Jacobian-based gradient descent approach is proposed. The Jacobian is found by vectorizing the analytical expression of $R^i_{i-1} \in \mathbb{R}^{3\times3}$ into $\hat{R}^i_{i-1} \in \mathbb{R}^9$ and by computing

$$J(\Delta x, \Delta y, \theta, g) = \frac{\partial \hat{R}^i_{i-1}}{\partial [\Delta x, \Delta y, \theta]^\top} \tag{8}$$

By computing the Jacobian, it is possible to minimize the displacement $\Delta R \in \mathbb{R}^9$ with respect to the manifold, evaluated as

$$\Delta R = \tilde{R}^i_{i-1} - R^i_{i-1}(\Delta x, \Delta y) R_{\text{drift}}(\theta) \tag{9}$$

To map the error in rotation ΔR into changes on the estimate of the shape $q = [\Delta x, \Delta y, \theta]$, the pseudoinverse of J is leveraged by iteratively update the estimate of the state with

$$\Delta q = \alpha J^\top \left(J J^\top\right)^{-1} \Delta R \tag{10}$$

where α is a gain. In the following, without loss of generality, α was set to 0.5. Note that within this gradient descent, the method estimates both the soft robot pose $\Delta x, \Delta y$ and the drift θ in the IMU. Refer to Algorithm 1 for a schematic overview of the filter steps.

IV. Simulation-Based Validation

Before validating the filter on a physical setup, the performance of the novel filter proposed was compared with state-of-the-art IMU-based algorithms, presented in [10]. To have a detailed analysis of the improvement achieved for different drift conditions and across the joint space, we simulated IMU data with different levels of drift, i.e. varying the value of θ in (5), for known $\bar{q} = [\Delta x, \Delta y]$ for a single segment. Hence

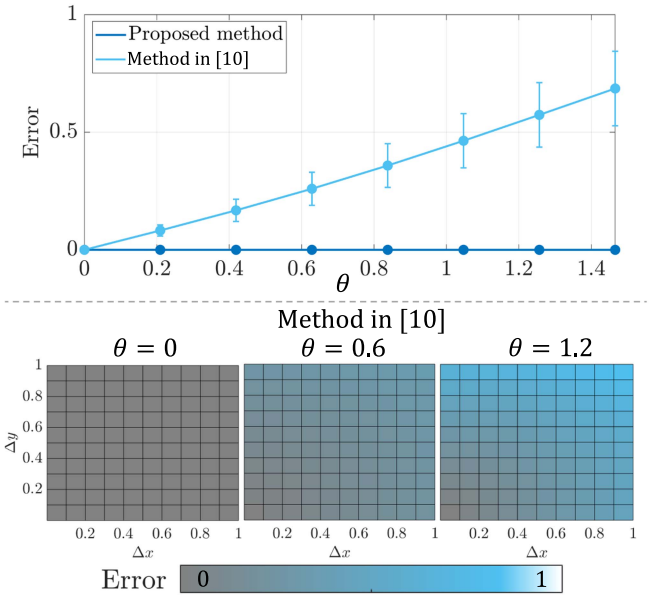

Fig. 6. On the top average error across the workspace, computed as mean(e) as a function of the imposed drift θ for the algorithms in [10], [14] against the proposed methodology. On the bottom, a heat map displaying the error across the PCC joint-space for the algorithm in [10]. As previous methods did not consider the drift effect, we observe an increase in error directly proportional to θ, which grows with the bending angles.

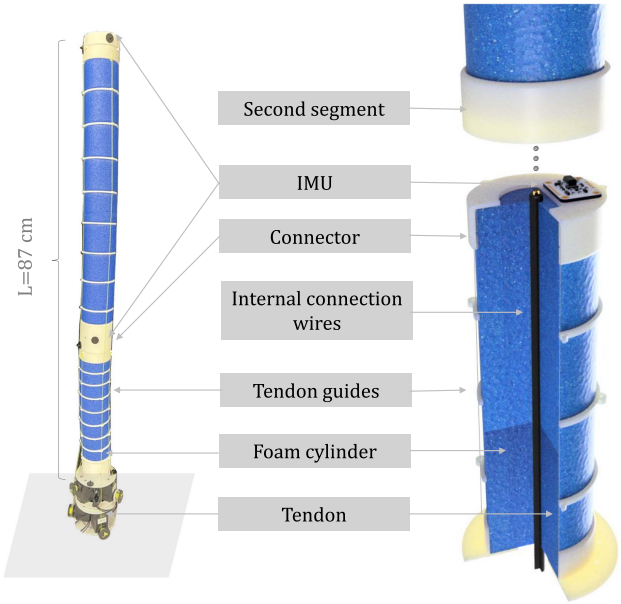

Fig. 7. Representation of the robotic structure. On the left, a photo of the real, bi-segment robot, while on the right a rendering of the cross-section view of a single segment of the robot. Each segment, composed of a foam cylinder is connected to subsequent segments through rigid connectors. The tendons are guided by 3D-printed holders, uniformly distributed along the length. A ribbon cable is routed through the center of the segment to provide signal and power to the IMU, placed at the junction between segments.

we performed the reconstruction of the soft robot shape with both the novel algorithm introduced in Section III-B and that presented in [10]. The error between the estimated state and $\bar{q}$ is finally computed, and the different algorithms are compared. Thanks to the simulated drifted data, it is possible to evaluate how the filter performs across the PCC joint space by sampling it with 100 samples per Lagrangian variable with several drift levels. In Fig. 6 we report the error in reconstruction for the different algorithms. As shown, in optimal conditions with no drift, both algorithms display no errors across the whole workspace. However, as soon as the drift is introduced, the reconstruction with the method presented in [10] shows an error of $0.6\sqrt{\Delta x^2 + \Delta y^2}$ across the joint space. Consequently, from simulation results, we demonstrate an improvement in accuracy of $0.6\sqrt{\Delta x^2 + \Delta y^2}$ with respect to state-of-the-art algorithms.

V. Real-World Validation

To validate the theory on a real system, a novel manipulator with embedded IMUs and a synchronized measurement system providing ground truth data is needed.

A. A Soft Robot With Embedded Proprioception

To validate the filter on a real system, we designed a novel manipulator with proprioceptive capabilities designed to match the constant curvature assumption behind this work. The soft robot structure comprises two cylindrical foam segments connected by 3D-printed holders. To enable real-world manipulation tasks, the robot was designed so to have a total length of 0.87 m with the attachment to the base, and 0.75 m not considering it. Thanks to the low density of the foam structure, the soft robot can self-support its own weight despite its large scale. An IMU (BNO055, Bosch, Adafruit) is attached to the connector glued at the end of each segment with the z axis parallel to the soft robot's longitudinal axis. The IMU represents the best performance for a consumer-grade device and allows for a fair comparison with existing works in the field [19]. A ribbon cable was routed through the center of the foam cylinder to transfer data and power between an Arduino UNO and the IMU. Note that in incompressible soft structures, the center of the segment does not change its length when deformed. In the following we consider this manipulator incompressible given the significantly high axial to bending stiffness ratio. Therefore the deformation capabilities are not affected by the routed internal wiring. Each segment is actuated by a set of three tendons attached to a motor at the base (Dynamixel XM430-W210 T) and to the respective tip of the segment. Ten 3D printed rings are placed regularly spaced along each foam cylinder to guide the tendon and distribute the tensile force into a constant moment along the compliant element [20]. The Arduino UNO and the motor controller are connected via serial to a main laptop, in which the IMU data are filtered, and the motor actions are computed in Matlab. Since each motor has built-in sensors, a control loop, and a profile generator, the motors can be used via position control, setting the lengths of tendons with a PCC forward kinematic mapping [17]. In Fig. 7 we report a render and a picture of the soft structure to display the different components of the soft manipulator. To ensure that data from both IMU and MoCap measurement systems are recorded synchronously, both systems' data is saved using a central Matlab algorithm script which imposes a stream rate of 20 Hz.

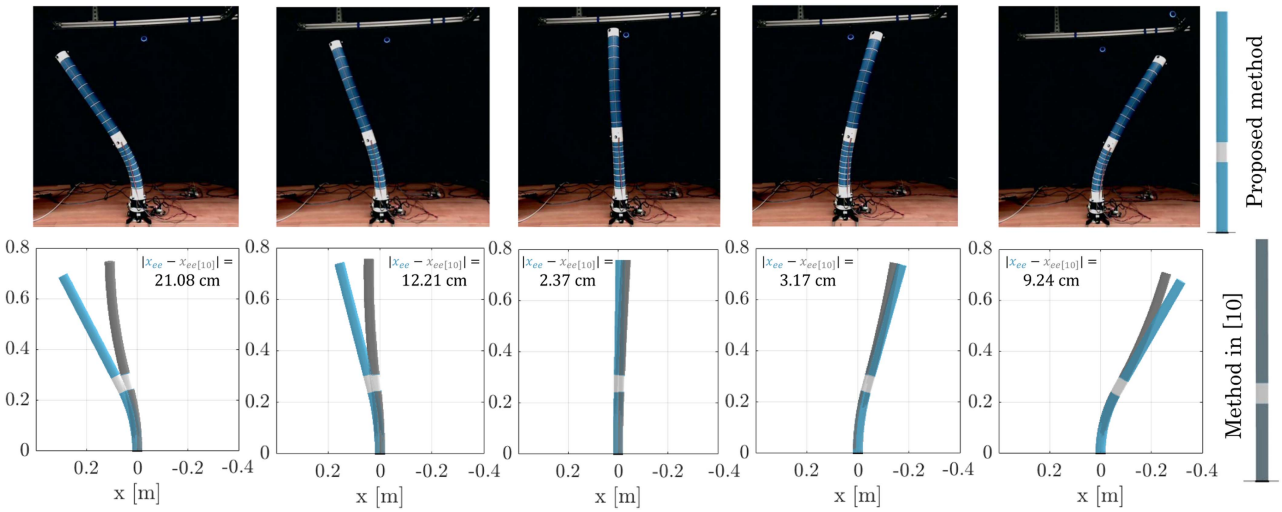

Fig. 8. Representation of the soft robot pose at $t = 15$ min for both the approach described in [10], in gray, and for the novel algorithm proposed in Section III-B, in blue. In agreement with the simulation, the error in reconstruction becomes more significant with the bending angle. The error in reconstruction for the same angle (e.g. extreme-right and extreme-left figures) of the method in [21] differs as the IMU drifted with different intensities in different recordings. In all of the recordings, the novel method shows a more accurate reconstruction of the soft robot state compared to state-of-the-art algorithms.

B. Ground-Truth Measurement System

A Motion Capture (MC) system (Optitrack) was used to benchmark the reconstruction accuracy of the filter. The system's accuracy is below 0.2 mm on position and below 0.05° on rotational error. The world frame of the motion capture was initially set so to match the world frame of the robotic system. Three triplets of markers are placed on the soft robot at the base, first connector and tip. Each set of markers was set as a rigid body to extract the position and orientation. Moreover, a camera was placed at a distance of 3 m from the manipulator to have images of the experiments to validate the results further. To further compensate for slight differences in orientation between the two systems, at the start of each experiment, the soft robot was placed in the straight configuration, and a calibration matrix R_{cal} was computed. To do so, it is imposed that at t_0 i.e. just after calibration, both the rotation matrix measured by the IMU $\tilde{R}_0^i$ and by the motion capture system R_{MC} are physically equal. Therefore, a misalignment of the two systems can be compensated with the relative rotation matrix $R_{\text{cal}} = \tilde{R}(t_0)^{-1} R_{\text{MC}}(t_0)$ Therefore, in each of the subsequent measurements, the IMU orientation was projected in the motion capture inertial frame by $\tilde{R}(t) = \tilde{R}(t)\tilde{R}(t_0)^{-1} R_{\text{MC}}(t_0)$. Finally, to compare the PCC reconstruction from the embedded IMUs, the Lagrangian PCC coordinates are computed with the inverse kinematic algorithm presented in [10].

VI. Experimental Results

In order to study the drift of the orientation measure provided by the IMU with respect to the drift-less one provided by the MC system, both long-term static and dynamical experiments were performed. Moreover, a third experiment in which the robot was externally perturbed (from a human) was performed to demonstrate the robustness to external disturbances. All the experiments and analyses have been performed on 3D trajectories. However, as the precision of the reconstruction is not influenced by the plane of deformation, we report planar movements for graphical clarity.

TABLE I
Error Between the Reconstructed Model and the Real Pose of the Soft Manipulator in the Static Case

Bending angle [°]	Segment 1		Segment 2	
	ΔR	Δx [cm]	ΔR	Δx [cm]
-30	0.19	3.1	0.18	6.3
-22.5	0.20	2.3	0.25	6.8
-15	0.18	1.9	0.14	4.4
-7.5	0.20	2.1	0.15	9.8
0	0.08	3.1	0.15	5.2
7.5	0.09	1.1	0.21	4.3
15	0.13	2.7	0.38	5.8
22.5	0.12	2.3	0.23	6.4
30	0.14	2.4	0.18	3.1

A. Static Experiment

In the static experiment show in Fig. 8 the soft manipulator was bent at several curvatures and angles, as to cover the whole workspace. The experiment was designed to observe and compensate for the drift appearing for some static shapes of the soft robot and to observe how it depends on the PCC parameters. Nine different static configurations were studied. In each configuration, the robot was kept static for 15 minutes. The IMUs were calibrated only at the start of the measurement resulting in a long-term 2.5 h continuous measurement of the soft robot's state. The performance in reconstruction was computed using the data at time $t = 15$min as both the Euclidean Cartesian distance of the reconstructed pose against the MC data as well as the Frobenius norm ΔR of distance between the MC rotation matrix and the filtered IMU data

$$\Delta R = \text{Frob}\left(R_{\text{IMU}}^{\top}(t) R_{\text{MC}}(t) - R_{\text{IMU}}^{\top}(t_0) R_{\text{MC}}(t_0)\right)$$

The novel filter shows an accuracy on the end effector pose of 93% of the robot's length. A detailed report of the errors for the different poses is provided in Table I.

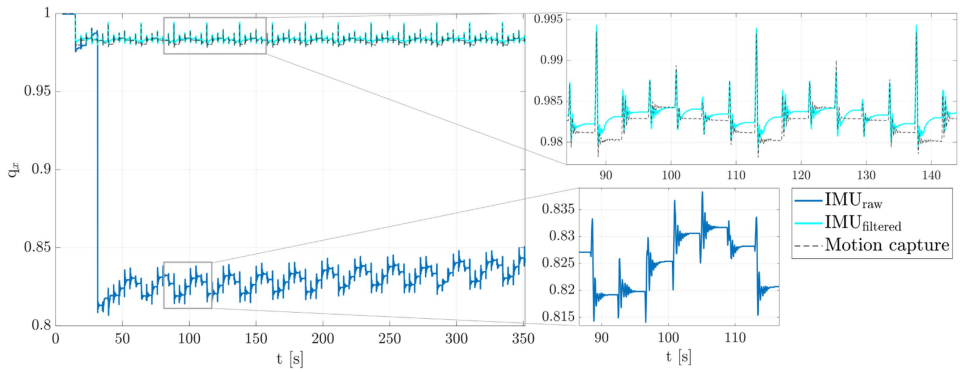

Fig. 9. On the left. the raw and filtered IMU signals, benchmarked with ground-truth data from the motion capture are shown. Notably, the filter can compensate for both the abrupt error happening at the start of the measurement and the long-term drift. On the right is a series of instances of the reconstructed 3D pose of the soft robot.

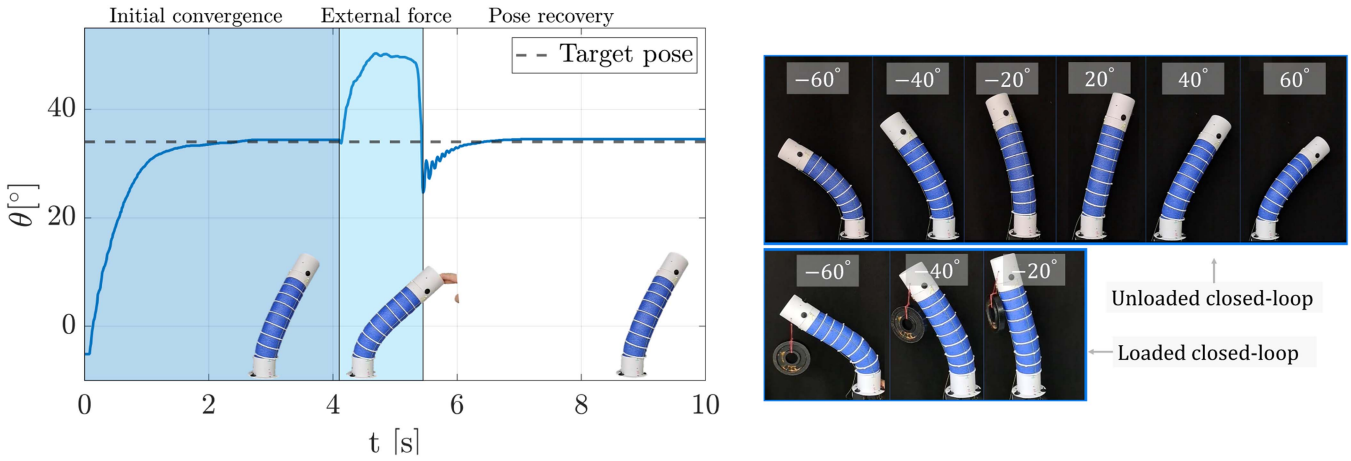

Fig. 10. On the left, the evolution of the signal for the target position $\theta = 37°$. Not only the robot steadily converges to the desired pose, but after an external perturbation recovers the pose without added error. On the right, it is possible to observe the convergence of the single segment to 6 different poses when controlled in closed-loop with IMU data. On the left-bottom, the reconstruction of 3 of the poses above when the robot is perturbed with an external load of 0.5 Kg. Notably, thanks to the closed-loop control, the robot can reach the same orientation of the tip by counterbalancing the load with control actions.

B. Dynamical Excitation

In the dynamical excitation experiment, the robot was moved sequentially between the poses described in Section VI-A with varying speeds. We report in Fig. 9 the reconstruction of the orientation signal in quaternion space, as well as a comparison with raw IMU signals. Notably, thanks to the high speed frequency of measurements, the high frequency oscillations of the system around the equilibrium pose are captured. This enforces the applicability of IMU-based reconstruction algorithms for dynamic, closed-loop, soft robot control.

VII. Closed-Loop Control

Thanks to the high frequency and accuracy of the reconstruction, the IMUs with the filter embedded in Algorithm 1 can be used to perform closed-loop control. In the following, we test this claim by using a closed-loop algorithm for a single segment of our robot with an IMU at the tip. More specifically, we use a classic actuation-level quasi-static kinematic inversion strategy [3, eq. (37)]. This algorithm relies on the hypothesis that a map $q = f(l)$ can be found that brings the actuator space, i.e. the cable lengths $l \in \mathbb{R}^3$, into configuration space q. Using these mapping $f(l)$ it can be computed the Jacobian of the robot as $J = [\partial f(l_1)/\partial l_1, \ldots \partial f(l_3)/\partial l_3]^\top$, where the tendon lengths are l_1, l_2, and l_3. The shape-control algorithm is

$$\dot{l} = \alpha J^+(l)(q_{\text{target}} - f(l)). \tag{11}$$

with q_{target} being the goal shape and α being a gain on the control inputs. In the following results, we used a gain of 2.

For the segment used here, the map f is among the ones introduced in [22] and it is so defined $L = \frac{l_1+l_2+l_3}{3}$, $\phi = \text{atan2}\left(\frac{\sqrt{3}(l_2+l_3-2l1)}{3(l_2-l_3)}\right)$, $\theta = \frac{2\sqrt{l_1^2+l_2^2+l_3^2-l_1l_2-l_1l_3-l_2l_3}}{d(l_1+l_2+l_3)}$, where L is the arc length, and d is the diameter of the section of the soft robot.

We map the Lagrangian coordinates from Δ-parametrization to ϕ-parametrization as described in [17]

$$\theta = \sqrt{\Delta x^2 + \Delta y^2},\ \phi = \text{acos}\left(\frac{\Delta x}{\sqrt{\Delta x^2 + \Delta y^2}}\right). \tag{12}$$

The angle θ is then used to compare the bending angle in the experiment represented in Fig. 10.

In Fig. 10, we show the convergence of this control scheme to the desired pose over 6 different bending angles. To further demonstrate the capabilities of this method, two experiments in which the robot was perturbed are reported. In the first experiment, shown in the bottom-left of Fig. 10, the soft robot was perturbed with a load of 0.5 Kg. Thanks to the closed loop shape control, the actuation forces compensate for the deformation arising. In the second experiment, the robot was manually deformed after the convergence of the controller. Notably, thanks to the embedded proprioception, the soft robot can compensate for the imposed displacement. Thanks to the high frequency of the IMU measurements, IMU-based reconstruction methods are a solution for the proprioception problem in soft robots undergoing dynamic interaction with the environment.

VIII. Conclusion

In this letter, a new kinematics-based filter for soft robot shape reconstruction was proposed. The filter exploits well-understood assumptions on the soft robot deformations to estimate and compensate for the drift occurring in Mahony-based estimations of IMUs postures. As a result, we could obtain stable and precise shape reconstructions. We evaluated the performance of the proposed algorithm in simulation and on a novel two-segment soft robot. The filter was bench-marked against state-of-the-art reconstruction algorithms for soft pose sensing. As a result, the proposed method achieves an accuracy on the end effector pose of 93% of the soft robot length. Concerning previous methods, this improvement in accuracy comes at the cost of a higher computational cost, which, however, does not limit the real-time applicability of the algorithm. We also preliminarily tested the proposed algorithm in closed-loop kinematic control. In the future, the kinematics-based reconstruction approach will be expanded to polynomial strain models [20], [23], [24] and embedded into modular elements [25] that can be placed on any soft robot. This will ultimately provide researchers with a much-needed method to capture and leverage the pose of soft slender robots in the interaction with the environment [26].

References

[1] D. Rus and M. T. Tolley, "Design, fabrication and control of soft robots," *Nature*, vol. 521, no. 7553, pp. 467–475, 2015.

[2] F. Stella and J. Hughes, "The science of soft robot design: A review of motivations, methods and enabling technologies," *Front. Robot. AI*, vol. 9, 2023, Art. no. 1059026.

[3] C. D. Santina, C. Duriez, and D. Rus, "Model-based control of soft robots: A survey of the state of the art and open challenges," *IEEE Control Syst. Mag.*, vol. 43, no. 3, pp. 30–65, Jun. 2023.

[4] H. Wang, M. Totaro, and L. Beccai, "Toward perceptive soft robots: Progress and challenges," *Adv. Sci.*, vol. 5, no. 9, 2018, Art. no. 1800541.

[5] A. Vicari et al., "Proprioceptive sensing of soft tentacles with model based reconstruction for controller optimization," in *Proc. IEEE Int. Conf. Soft Robot.*, 2023, pp. 1–6.

[6] T. Baaij et al., "Learning 3D shape proprioception for continuum soft robots with multiple magnetic sensors," *Soft Matter*, vol. 19, pp. 44–56, 2022.

[7] R. L. Truby, C. D. Santina, and D. Rus, "Distributed proprioception of 3D configuration in soft, sensorized robots via deep learning," *IEEE Robot. Automat. Lett.*, vol. 5, no. 2, pp. 3299–3306, Apr. 2020.

[8] J. L. Molnar, C.-A. Cheng, L. O. Tiziani, B. Boots, and F. L. Hammond, "Optical sensing and control methods for soft pneumatically actuated robotic manipulators," in *Proc. IEEE Int. Conf. Robot. Automat.*, 2018, pp. 3355–3362.

[9] E. R. Rosi, M. Stölzle, F. Solari, and C. Della Santina, "Sensing soft robots' shape with cameras: An investigation on kinematics-aware SLAM," in *Proc. IEEE 5th Int. Conf. Soft Robot.*, 2022, pp. 795–801.

[10] J. Hughes, F. Stella, C. D. Santina, and D. Rus, "Sensing soft robot shape using IMUs: An experimental investigation," in *Proc. 17th Int. Symp. Exp. Robot.*, 2020, pp. 543–552.

[11] B. G. Cangan, S. E. Navarro, B. Yang, Y. Zhang, C. Duriez, and R. K. Katzschmann, "Model-based disturbance estimation for a fiber-reinforced soft manipulator using orientation sensing," in *Proc. IEEE/RSJ Int. Conf. Intell. Robots Syst.*, 2022, pp. 9424–9430.

[12] H. Bezawada, C. Woods, and V. Vikas, "Shape reconstruction of soft manipulators using vision and IMU feedback," *IEEE Robot. Automat. Lett.*, vol. 7, no. 4, pp. 9589–9596, Oct. 2022.

[13] K. Stewart, Z. Qiao, and W. Zhang, "State estimation and control with a robust extended Kalman filter for a fabric soft robot," *IFAC-PapersOnLine*, vol. 55, no. 37, pp. 25–30, 2022.

[14] Y. J. Martin, D. Bruder, and R. J. Wood, "A proprioceptive method for soft robots using inertial measurement units," in *Proc. IEEE/RSJ Int. Conf. Intell. Robots Syst.*, 2022, pp. 9379–9384.

[15] C. Armanini, F. Boyer, A. T. Mathew, C. Duriez, and F. Renda, "Soft robots modeling: A structured overview," *IEEE Trans. Robot.*, vol. 39, no. 3, pp. 1728–1748, Jun. 2023.

[16] R. Mahony, T. Hamel, and J.-M. Pflimlin, "Nonlinear complementary filters on the special orthogonal group," *IEEE Trans. Autom. Control*, vol. 53, no. 5, pp. 1203–1218, Jun. 2008.

[17] C. D. Santina, A. Bicchi, and D. Rus, "On an improved state parametrization for soft robots with piecewise constant curvature and its use in model based control," *IEEE Robot. Automat. Lett.*, vol. 5, no. 2, pp. 1001–1008, Apr. 2020.

[18] R. Mahony, V. Kumar, and P. Corke, "Multirotor aerial vehicles: Modeling, estimation, and control of quadrotor," *IEEE Robot. Automat. Mag.*, vol. 19, no. 3, pp. 20–32, Sep. 2012.

[19] Z. Lin, Y. Xiong, H. Dai, and X. Xia, "An experimental performance evaluation of the orientation accuracy of four nine-axis MEMS motion sensors," in *Proc. IEEE 5th Int. Conf. Enterprise Syst.*, 2017, pp. 185–189.

[20] F. Stella, Q. Guan, C. D. Santina, and J. Hughes, "Piecewise affine curvature model: A reduced-order model for soft robot-environment interaction beyond PCC," in *Proc. IEEE Int. Conf. Soft Robot.*, 2023, pp. 1–7.

[21] J. Hughes, C. D. Santina, and D. Rus, "Extensible high force manipulator for complex exploration," in *Proc. IEEE 3rd Int. Conf. Soft Robot.*, 2020, pp. 733–739.

[22] R. J. Webster III and B. A. Jones, "Design and kinematic modeling of constant curvature continuum robots: A review," *Int. J. Robot. Res.*, vol. 29, no. 13, pp. 1661–1683, 2010.

[23] C. D. Santina and D. Rus, "Control oriented modeling of soft robots: The polynomial curvature case," *IEEE Robot. Automat. Lett.*, vol. 5, no. 2, pp. 290–298, Apr. 2020.

[24] F. Stella, N. Obayashi, C. D. Santina, and J. Hughes, "An experimental validation of the polynomial curvature model: Identification and optimal control of a soft underwater tentacle," *IEEE Robot. Automat. Lett.*, vol. 7, no. 4, pp. 11410–11417, Oct. 2022.

[25] Q. Guan, F. Stella, C. D. Santina, J. Leng, and J. Hughes, "Trimmed helicoids: An architectured soft structure yielding soft robots with high precision, large workspace, and compliant interactions," *npj Robot.*, vol. 1, no. 1, 2023, Art. no. 4.

[26] F. Stella, J. Hughes, D. Rus, and C. D. Santina, "Prescribing cartesian stiffness of soft robots by co-optimization of shape and segment-level stiffness," *Soft Robot.*, vol. 10, pp. 701–712, 2023.